Iraqi Journal of Physics, 2024 *Vol. 22, No. 1, PP. 20-30*

https://doi.org/10.30723/ijp.v22i1.1174 *P-ISSN: 2070-4003*
E-ISSN: 2664-5548

Synthesis and Characterization of Aluminum Oxide Nanoparticles Prepared by Two Different Cold Plasma Jet Methods

Abdulrhman H. Shaker[1a*] and Kadhim A. Aadim[1b]
[1]*Department of Physics, College of Science, University of Baghdad, Baghdad, Iraq*
[b]E-mail: kadhim.aadim@sc.uobaghdad.edu.iq
[a*]Corresponding author: abd.hamed2204m@sc.uobaghdad.edu.iq
Dr. Kadhim A. Aadim is an editor position within the journal for the journal but did not participate in the peer review process other than as an author. The authors declare no other conflict of interest.

Abstract

In this paper, a cold plasma system utilizing a high voltage of 13.5 kV of alternative (AC) and direct current (DC) was used under atmospheric pressure with argon (Ar)-gas at a flow rate of 2.5 l/min and a flowing time of 4 min to synthesize aluminum oxide (AlO) nanoparticles (NP). From the results, when DC was used, it was found that the absorption spectrum starts at 303 nm and gradually falls to 870 nm. With AC, the absorption spectrum was at 330 nm and then began to fall to 902 nm. The energy gap when utilizing DC and AC was 3.49 and 3.44 eV respectively. The analysis of the X-ray diffraction (XRD) patterns showed the structure of the NPs was amorphous, matching the pattern 42-1746. At DC, the average size of NPs formed, as deduced from the XRD pattern, was 29.56 nm, and it was very close to what appeared in the field emission scanning electron microscopy (FESEM) images, in which the apparent NP size ranged between 20 and 50 nm. The XRD test gave an average NP size of 38.21 nm in AC, while the FESEM images showed a size range of 20-60 nm. At dc, the AlO NPs were aggregated and interconnected, and each set was connected to another set, as shown in the FESEM images. At AC, the shape of the synthesized AlO NPs was quasi-spherical, with slightly elongated particles connected.

Article Info.

Keywords:
Non-Thermal Plasma, AlO Nanoparticle, Plasma Jet, AC DC Cold Plasma, FESEM.

Article history:
Received: Jul 17, 2023
Revised: Sep 18, 2023
Accepted: Sep 28, 2023
Published: Mar 01,2024

1. Introduction

Plasma-liquid interaction has drawn much interest as a cutting-edge method for producing nanoparticles [1-3]. The direct reduction of metal ions in the gas-liquid interface can be started by electrons, with energy as high as a few electron volts, produced by atmospheric pressure plasma [4-6]. Nanoparticles may be created using a variety of plasma types [7, 8]: (a) direct plasma, like a gas discharge between the electrodes, and (b) remote plasma or plasma jet, a gas discharge between an electrode and the electrolyte surface. The plasma often acts as the cathode [9-12]. Atmospheric pressure plasma operating at room temperature has attracted great interest due to its ease of scaling up, low cost, and small size [13, 14]. The plasma column produced in the plasma jet system can be used for direct treatment without restriction of body size in medical subjects. Plasma jets are useful for more industrial applications because of their ability to scale up [15-18].

Several important new-century technologies depend increasingly on nanotechnology. A growing field of nanoscience and nanotechnology uses nano-scale materials and structures, typically measuring between (1 - 100) nm [19]. Many studies have been published on the manufacture and uses of metal nanoparticles because they exhibit unique features compared to their bulk counterparts [20, 21]. Earlier formulations of energetic materials frequently employ some of these metals, especially aluminum. Several companies, including those that produce explosives and pyrotechnic

propellants, are interested in aluminum oxide nanoparticles (AlO NPs). A variety of these compositions have had aluminum powder added to them to improve performance by boosting reaction energies, flame temperatures, and blast speeds. AlO NPs are more advantageous due to their high enthalpy of combustion and quick kinetics, which further enhance these reaction properties [22-24].

AlO NPs are recognized as a novel energetic material with extremely high reactivity due to their enormous specific surface area. The diameter of an AlO NP affects its reactivity. The most sensitive AlO NPs are said to be between 30 and 50 nm in size [25-27]. Aluminum's physical and chemical characteristics, especially those of its NPs, such as their corrosion-resistant and conductivity, make them suitable for use in a wide range of applications, including alloy powder metallurgy parts for cars and airplanes, heat-shielding coatings for aircraft and heat-reflecting paints, decorative plastics, soldering and termite welding, pyrotechnics, and military uses (rocket fuel, igniter, smokes, and tracers). AlO NPs are being researched as high-capacity hydrogen storage materials at the nanoscale level [28-31]. The cold plasma jet is one of the most effective redox methods for the production of nanoparticles. Gas exposed to a high electric field to be electrically charged is called a non-thermal plasma jet. Most of the energy from the electric field is utilized to produce active plasma species rather than merely heating the gas [15]. These species are made up of electromagnetic radiation, electrically neutral gas atoms, molecules, free radicals, positive ions, electrons, and negative ions. When aluminum is immersed in ionized water, plasma species, which are strong oxidizers, effect on the metal's surface. The metal's surface gets oxidized [32-35].

In this study, the NPs were prepared by a technique based on a cold plasma jet under atmospheric pressure generated from argon (Ar)-gas employing a voltage power supply of alternating current (AC) and then with a continuous current (DC) that directly interacts with liquid in which a piece of Al was immersed in deionized water. A flow of Ar gas was applied towards the surface of the liquid, producing a reaction that resulted in the production of AlO NPs.

2. Experimental Work

Cold plasma jet technology based on atmospheric pressure was constructed using an Al plate with a purity of 99.99%, Ar-gas with a flow rate of 2.5 l/min and a power supply supplying 13 kV. A plasma jet system that produced the cold plasma from argon gas synthesized Al NPs. Ar gas flows through a hollow metal tube with a diameter of 3 mm connected to a gauge that measures the amount of gas entering. In the system, an Al metal plate with dimensions (6 x 1) cm was placed in a small beaker containing ionized water. 4 cm of the metal plate was immersed in water, which was connected to a high-voltage power supply as the positive electrode (anode), while the electrically conductive end of the hollow metal tube through which the argon gas flows was connected to a high-voltage power supply as the negative electrode (cathode). The conductive end of the cathode (of a needle shape) was placed at a distance of 1 cm from the surface of the water. Ar gas flows at a rate of 2.5 l/min for 4 min over the water surface. With the flow rate and applied voltage fixed, the system was first operated with an alternating current (AC) and then with a continuous current (DC). After more than a minute, the impurities began to increase, and the color of the water started to change gradually to turn white.

The system was constructed using an Ar-gas bottle, which was connected to the negative end of the current power supply and flowed in the direction of the Al plate that was submerged in the water, which was connected to the positive end of the current power supply, which represents the positive pole. Fig. 1 shows the cold plasma jet system setup with a schematic diagram.

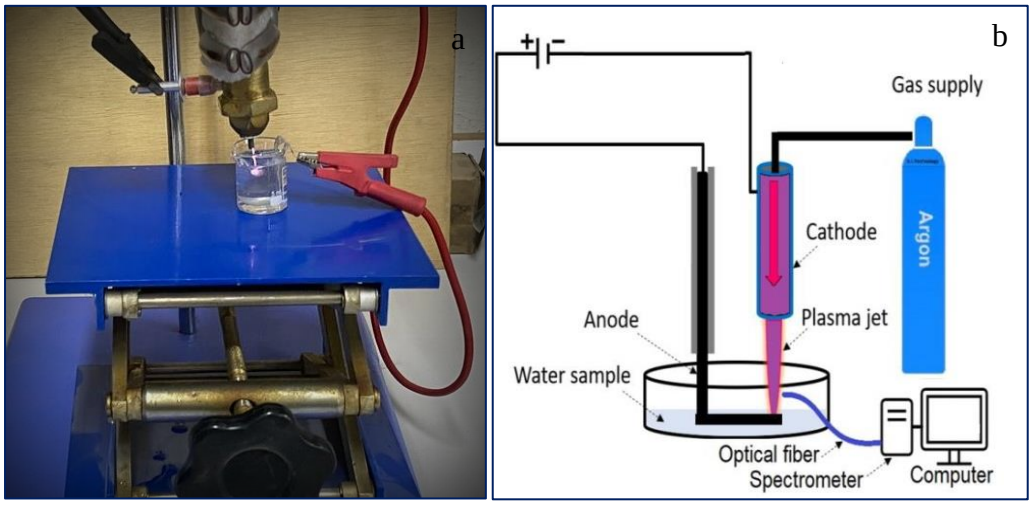

Figure 1: (a) the setup and (b) a schematic diagram of the cold plasma jet system.

3. Result and Discussion

After the synthesis process an ionized liquid containing AlO NPs was obtained, which was white in color, as shown in Fig. 2.

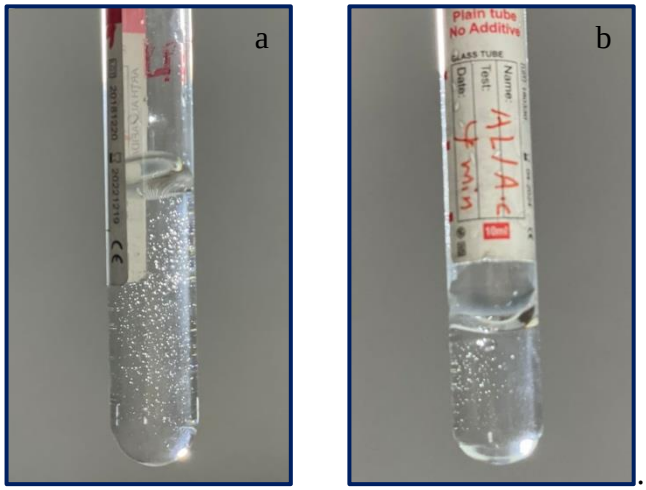

Figure 2: The AlO NPs using (a) DC and (b) AC Power Supply.

3.1. Optical Characteristics of AlO NPs Produced by Plasma Using an DC Power Supply

3.1.1. Absorption Coefficients and Absorbance

The absorption coefficient (α) of AlO NPs thin film was calculated using [36]:

$$\alpha = 2.303\frac{A}{t} \qquad (1)$$

where: A is the absorbance, and t is the thickness of the thin film.

Fig. 3 displays the fluctuation of the absorbance of the nanoparticles with wavelength.

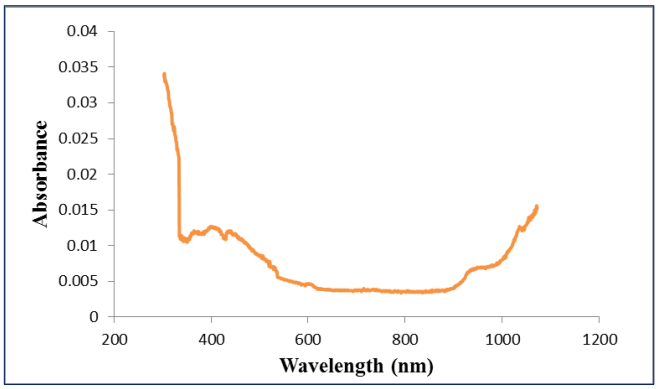

Figure 3: Absorbance as a function of wavelength for AlO NPs produced by (DC) cold plasma jet.

To identify the type of transition between the valence band and the conduction band, the connection between $(\alpha h\nu)^{1/r}$ and the photon energy ($h\nu$) for values of (r) was examined [37, 38].

$$(\alpha h\nu) \approx \left(h\nu - E_g\right)^r \qquad (2)$$

where (h) is the Plank constant, (ν) represents the frequency of the incident photon, E_g is the optical energy gap, and (r) is the optical transmission mode and represents a fixed value according to the type of transition, for example when r = 1/2, the mode of transition is directly allowed, and when r = 3/2, there is no possibility of moving directly at all, and when r = 2 the transition is indirectly allowed, but when r = 3 it prevents indirect transmission. The optical energy gap was determined by plotting $(\alpha h\nu)^2$ versus the photon energy and extrapolating the linear portion of $(\alpha h\nu)^2$ and $(\alpha h\nu)^{3/2}$ [38].

From Fig. 4, it was found that the value of the energy gap was 3.49 eV. The practical value matched the theoretical value of the energy gap when a DC was used in the non-thermal plasma system. This energy gap value was close to the values found by other works [39, 40].

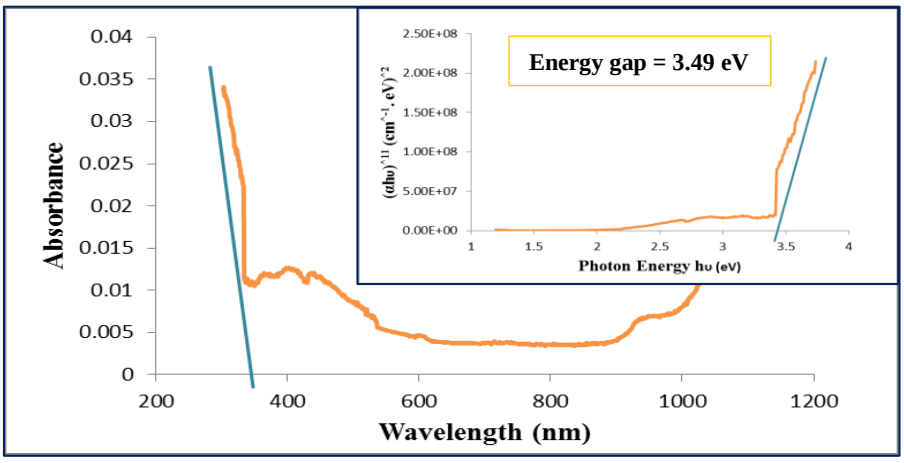

Figure 4: Value of E_g in a plot of $(\alpha h\nu)^2$ versus ($h\nu$) of AlO NPs using DC cold plasma.

3.1.2. XRD Characterization of AlO NPs

The AlO NPs thin films samples were examined with an XRD (Phillips, X-Pert PA analytical, Holland). It was found that the XRD pattern, shown in Fig.5, for the AlO NPs produced using direct current, matched the pattern in No: 00-004-07870 [41]. Weak absorption peaks were noted at 2θ of 21.66, 22.66, 28, 15, 30.15, 33.25, 57.05, and 77.25, noting that the average size of NPs formed was equal to 29.56 nm.

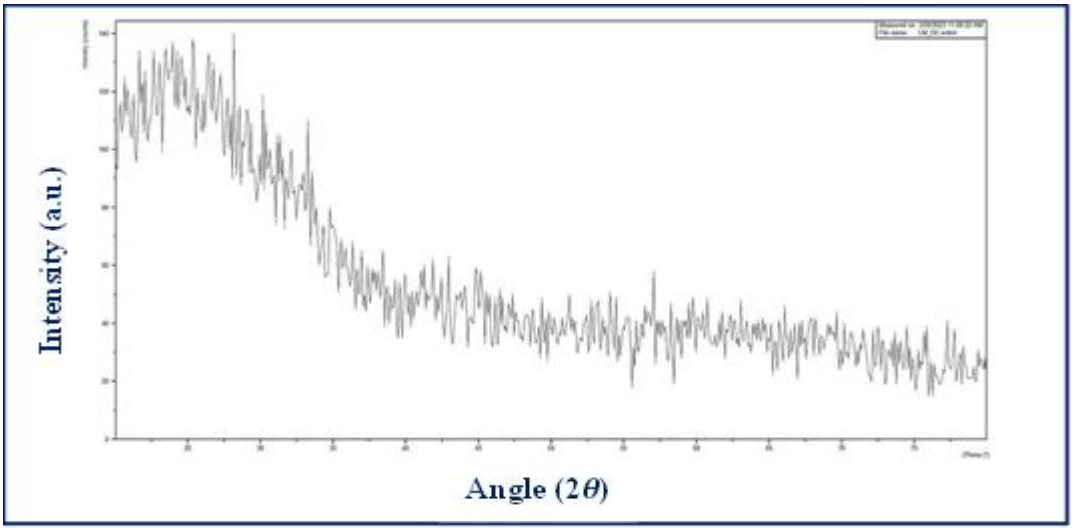

Figure 5: XRD pattern of AlO NPs produced by DC cold plasma at 4 min with an applied voltage of 13 kV.

3.1.3. Characterization of AlO NPs by FESEM

The obtained FESEM images of AlO NPs, as shown in Fig.(6 a,b), show the NPs to be in the form of interconnected ramifications. The images, at 200 nm scale, showed spheres aggregated and connected to each other, and each set of spheres is connected to another set to form a tangle of nanoparticles. The images were almost identical to those of Khodadadi et al. [42].

Fig. (6 a, b) shows that AlO NPs have a diameter ranging between 20 and 50 nm according to the used scale. This result agreed with the NPs average size of 29.56 nm obtained with XRD study. The variation in the particles diameter and, thus, their sizes can be explained due to the effect of the Ar flowing time on the surface of the liquid in which the metal piece of aluminum was immersed, which was a maximum of 4 min.

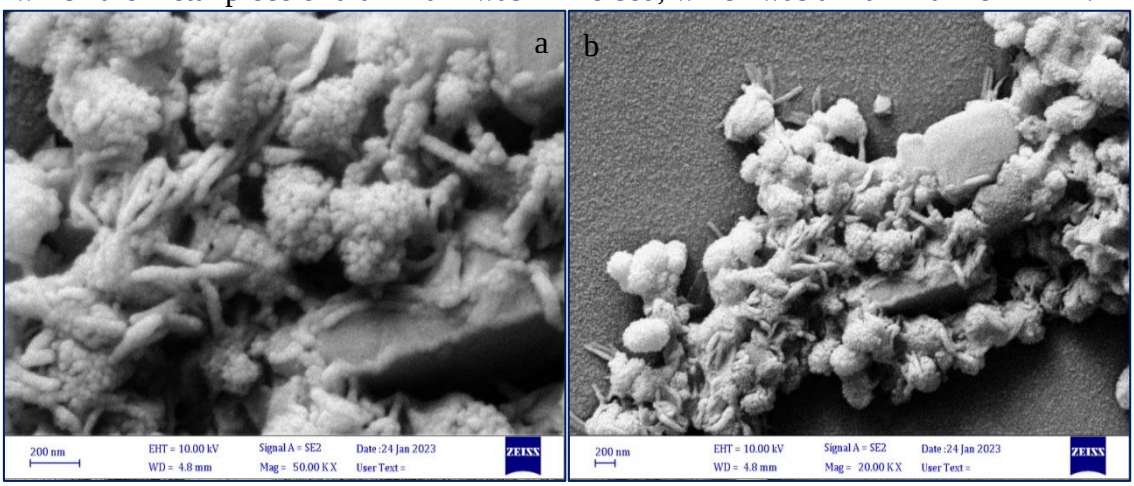

Figure (6): FESEM images at 200 nm scale of AlO NPs produced by cold plasma jet using DC.

Fig. 7, the nano-scale dendrites of the aluminum metal were like balls, such as granules, connected to each other. Through the EDS study, it was found that the percentage of aluminum metal in AlO NPs was 55.4% and the percentage of oxygen gas was 44.6%.

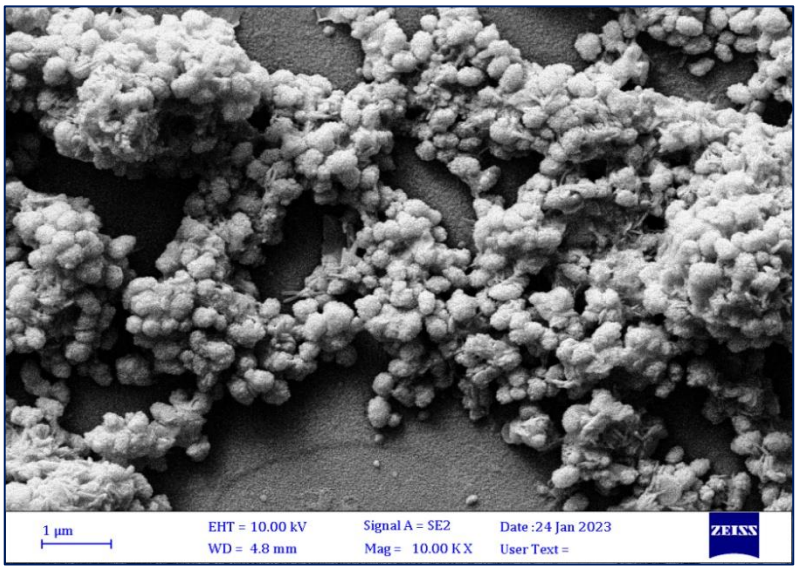

Figure 7: FESEM image at 1 µm scale of AlO NPs generated by cold plasma jet using DC.

3.2. Optical Characteristics of AlO NPs Produced by Plasma Using an AC Power Supply

3.2.1. Absorption Coefficients and Absorbance

Eq.1 was used to obtain the absorption coefficient from the largest absorption area near the basic absorption edge of the nano unit. Fig. 8 displays the changes of absorbance with wavelength generated by the AC plasma jet. It is clear that the absorbance spectrum of AlO NPs produced using a cold plasma jet generated with an AC power supply is the same as that of the nanoparticles produced using plasma generated with a DC power supply.

The value of the energy gap, in this case, was 3.44 eV, as shown in Fig. 9, which is close to the values of the energy gap found in Zhang et.al, Sokoloff et.al and Peng [43-45].

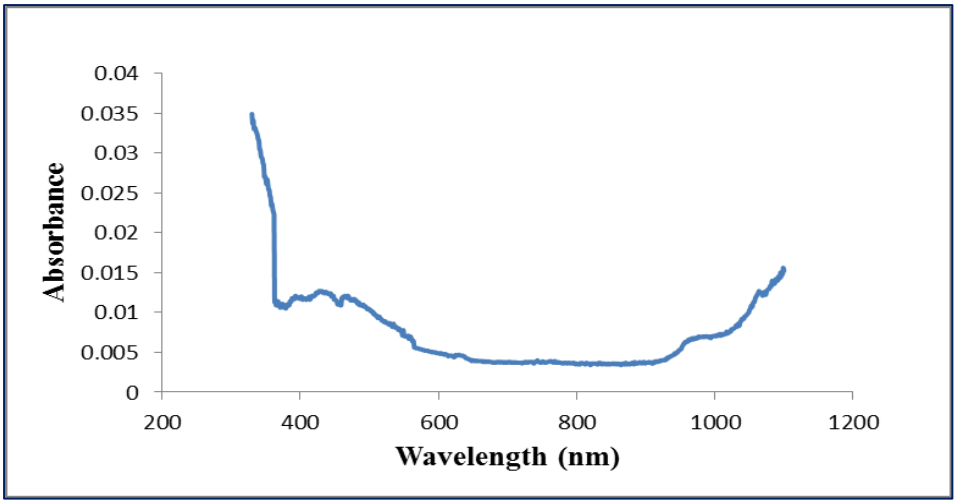

Figure 8: Absorbance as a function of wavelength for AlO NPs liquid produced by AC plasma jet measured by UV-visible.

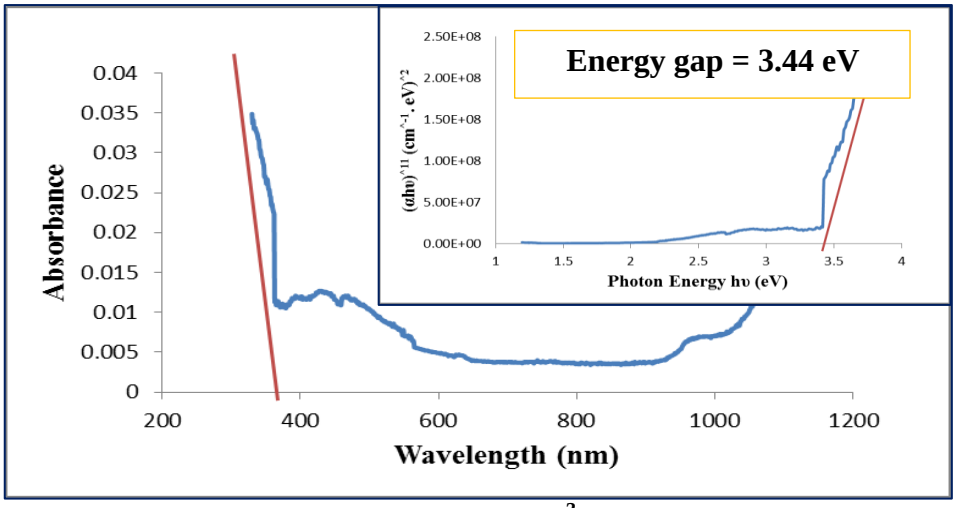

Figure 9: The value of E_g in a plot of $(\alpha h\upsilon)^2$ versus $(h\upsilon)$ of AlO NPs using (AC) cold plasma.

3.2.2. Characterization of AlO NPs by XRD

The XRD pattern of AlO NPs using AC, Fig. 10, shows that the NPs are of amorphous nature. This pattern matched that in No: 00-004-07870) [46]. The average size of the formed nanoparticles was found to be 38.21 nm.

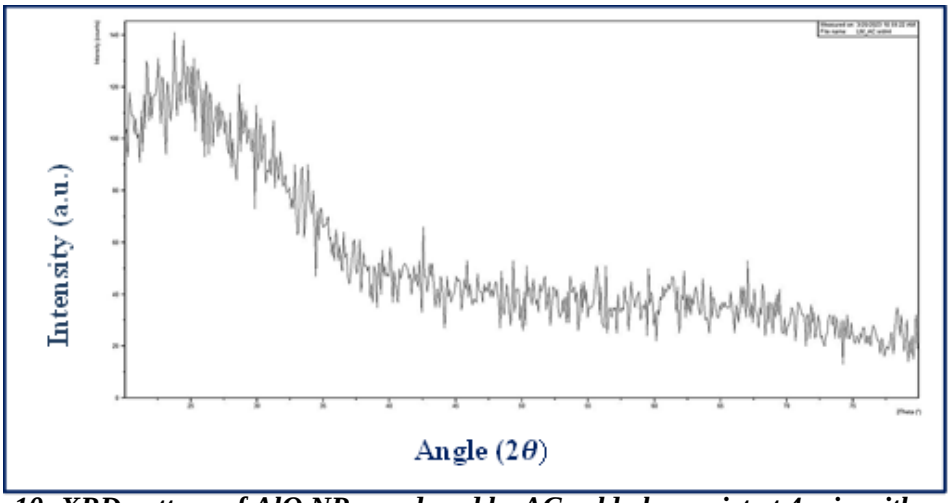

Figure 10: XRD pattern of AlO NPs produced by AC cold plasma jet at 4 min with an applied voltage of 13 kV.

3.2.3. Characterization of AlO NPs by FESEM

AlO NPs produced by the cold plasma jet generated using AC differed from those produced by DC, as noted from the FESEM images, shown in Figs. 11 and 12. The images at 1µm scale showed a series of particles connected to each other and intertwined as if they were sticky.

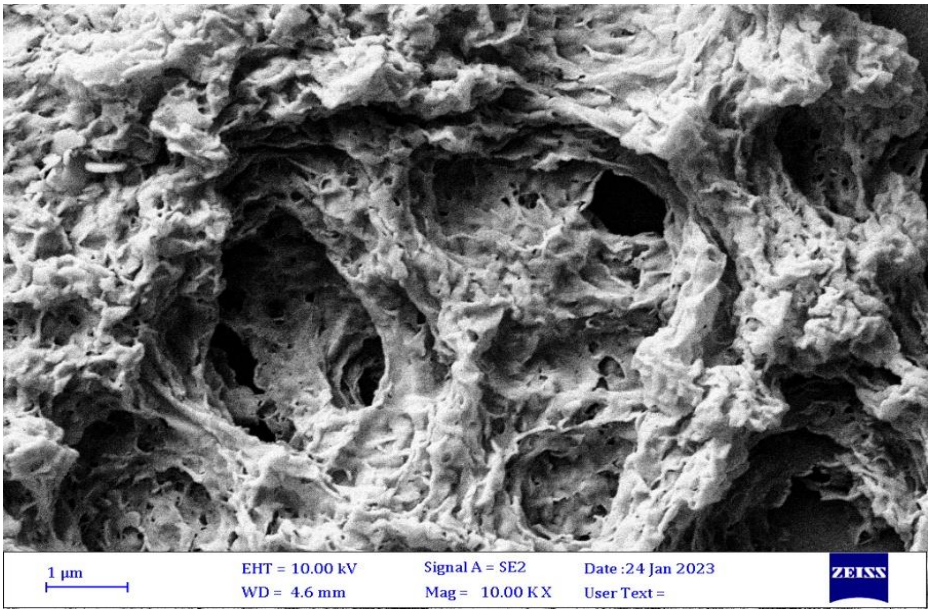

Figure 11: FESEM image at 1 µm scale of AlO NPs generated by non-thermal plasma jet.

The FESEM images at 1 µm scale show that each particle was semi-spherical inclined to be slightly elongated and connected to each other to be more like a gelatinous substance and knitted together like scattered wool.

Fig. 12 shows the FESEM image of AlO NPs generated from the plasma at a voltage of 13 kV AC have NPs size in the range (20 - 60) nm. This result agrees with the NPs average size of 29.56 nm obtained with the XRD study. Through the EDS study, it was found that the percentage of aluminum metal in nanosized aluminum was 47.2%, and the percentage of oxygen gas was 52.8%. The shape is almost close to the FESEM images in the study of Yousef et al. [47].

The diameter of the particles explains their sizes as due to the time that the plasma hits the surface of the water, which was a maximum of 4 min [48, 49].

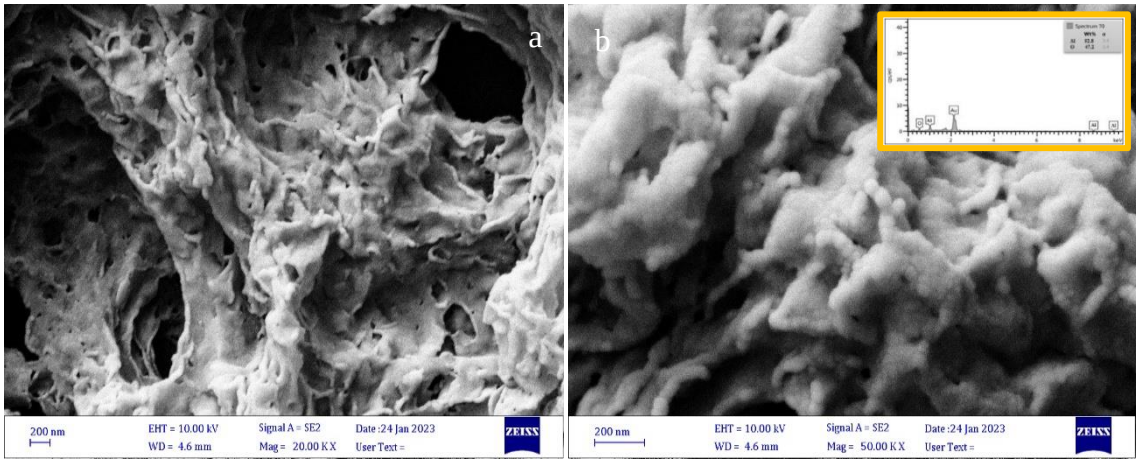

Figure 12: FESEM image (at 200 nm scale) of AlO NPs generated by non-thermal plasma jet using AC.

4. Conclusions

The color of the synthesized nanofluid using the two types of cold plasma currents was similar. At DC with a constant high voltage of 13 kV and Ar-gas flow rate of 2.5 L/min for 4 min, AlO NPs were synthesized. The absorption spectrum was higher in DC than in AC and the E_g value when using DC was higher than in AC. The XRD analysis of AlO NPs produced using DC and AC in plasma jet showed that the NPs were amorphous, which means all peaks were somewhat weak and not high in both DC and AC, and the size of AlO NPs was smaller in DC than in AC. In FESEM images of DC, the general shape of the NPs was a group of balls interconnected with another group to form a tangle of particle nanoparticles of AlO NPs. As for the shape of a single particle, it is irregular, longitudinal, and tends to be cylindrical, while in AC the shape of the nanoparticles, as seen in the FESEM images, was a series of particles connected and intertwined as if they were glue stocked. The shape of the particle was almost spherical tending to be slightly elongated and joined together to be more like a gelatinous substance and held together like scattered wool.

Conflict of interest

Authors declare that they have no conflict of interest.

References

1. O. L. Li, H. Lee, and T. Ishizaki, Japanese J. Appl. Phys. **57**, 0102A2 (2018).
2. K. Pal, A. Si, G. S. El-Sayyad, M. A. Elkodous, R. Kumar, A. I. El-Batal, S. Kralj, and S. Thomas, Crit. Rev. Sol. Stat. Mat. Sci. **46**, 385 (2021).
3. C. Ma, A. Nikiforov, N. De Geyter, R. Morent, and K. K. Ostrikov, Cur. Opin. Chem. Eng. **36**, 100764 (2022).
4. S. Wang, K. Qian, X. Bi, and W. Huang, J. Phys. Chem. C **113**, 6505 (2009).
5. D. T. Elg, H. E. Delgado, D. C. Martin, R. M. Sankaran, P. Rumbach, D. M. Bartels, and D. B. Go, Spectrochim. Acta Part B: Atom. Spectro. **186**, 106307 (2021).
6. P. Xie, Y. Qi, R. Wang, J. Wu, and X. Li, Nanomaterials **9**, 1488 (2019).
7. G. Saito and T. Akiyama, J. Nanomater. **16**, 299 (2016).
8. P. Jawaid, M. U. Rehman, Q.-L. Zhao, M. Misawa, K. Ishikawa, M. Hori, T. Shimizu, J.-I. Saitoh, K. Noguchi, and T. Kondo, Cell Death Discov. **6**, 83 (2020).
9. R. Wang, S. Zuo, W. Zhu, J. Zhang, and J. Fang, Plasma Proces. Poly. **11**, 448 (2014).
10. Y. Zhang, J. Liu, X. Mao, G. Chen, and D. Tian, Tr. Analyt. Chem. **144**, 116437 (2021).
11. A. Thiha, F. Ibrahim, S. Muniandy, and M. J. Madou, Microsys. Nanoeng. **5**, 62 (2019).
12. M. S. Simeni, Y. Zheng, E. V. Barnat, and P. J. Bruggeman, Plasma Sour. Sci. Tech. **30**, 055004 (2021).
13. S. Wu, F. Wu, C. Liu, X. Liu, Y. Chen, T. Shao, and C. Zhang, Plasma Proce. Poly. **16**, 1800176 (2019).
14. L. Di, Z. Zhan, X. Zhang, B. Qi, and W. Xu, Plasma Sci. Tech. **18**, 544 (2016).
15. D. Braný, D. Dvorská, E. Halašová, and H. Škovierová, Int. J. Molecu. Sci. **21**, 2932 (2020).
16. A. Rabinovich, G. Nirenberg, S. Kocagoz, M. Surace, C. Sales, and A. Fridman, Plasma Chem. Plasma Proces. **42**, 35 (2022).
17. T. M. C. Nishime, R. Wagner, and K. G. Kostov, Polymers **12**, 1028 (2020).

18. U. Roobab, X.-A. Zeng, W. Ahmed, G. M. Madni, M. F. Manzoor, and R. M. Aadil, MDPI Foods **12**, 710 (2023).
19. J. Benedikt, H. Kersten, and A. Piel, Plasma Sour. Sci. Tech. **30**, 033001 (2021).
20. S. Chandra, A. Kumar, and P. K. Tomar, Spectrochim. Acta Part A: Mole. Biomole. Spectros. **92**, 392 (2012).
21. K. A. Aadim and A. S. Jasim, Karbala Int. J. Mod. Sci. **8**, 71 (2022).
22. M. Shariat, Optik **277**, 170698 (2023).
23. F. Siddique, S. Gonzalez-Cortes, A. Mirzaei, T. Xiao, M. Rafiq, and X. Zhang, Nanoscale **14**, 11806 (2022).
24. E. Carlos, R. Martins, E. Fortunato, and R. Branquinho, Chem.-A Euro. J. **26**, 9099 (2020).
25. J. L. Hueso, R. Mallada, and J. Santamaria, Cataly. Today **423**, 113927 (2023).
26. K. Zhang, R. A. Ganeev, G. S. Boltaev, and C. Guo, Appl. Phys. A **125**, 698 (2019).
27. Y. Li, R. K. Kalia, A. Nakano, and P. Vashishta, J. Appl. Phys. **114**, 134312 (2013).
28. F. Imam, N. O. Al-Harbi, M. M. Al-Harbia, H. M. Korashy, M. A. Ansari, M. M. Sayed-Ahmed, M. N. Nagi, M. Iqbal, M. Khalid Anwer, I. Kazmi, M. Afzal, and S. Bahashwan, Cardiovas. Toxicol. **17**, 58 (2017).
29. H. Li, M. J. Meziani, F. Lu, C. E. Bunker, E. A. Guliants, and Y.-P. Sun, J. Phys. Chem.y C **113**, 20539 (2009).
30. X. Ke, G. P. Howard, H. Tang, B. Cheng, M. T. Saung, J. L. Santos, and H.-Q. Mao, Advan. Drug Deliv. Rev. **151-152**, 72 (2019).
31. K. Wang, H. Jiang, Q. Wang, B. Ye, and W. Ding, Metallur. Mat. Trans. A **47**, 4788 (2016).
32. M. Domonkos, P. Tichá, J. Trejbal, and P. Demo, MDPI Appl. Sci. **11**, 4809 (2021).
33. J.-W. Lackmann and J. E. Bandow, Appl. Microbio. Biotech. **98**, 6205 (2014).
34. M. F. Kotkata, F. A. Abdel-Wahab, and M. S. Al-Kotb, Appl. Surf. Sci. **255**, 9071 (2009).
35. D. S. Kharitonov, J. Sommertune, C. Örnek, J. Ryl, I. I. Kurilo, P. M. Claesson, and J. Pan, Corros. Sci. **148**, 237 (2019).
36. L. J. Fu, H. Liu, C. Li, Y. P. Wu, E. Rahm, R. Holze, and H. Q. Wu, Sol. Stat. Sci. **8**, 113 (2006).
37. I. K. Abbas and K. A. Aadim, Sci. Tech. Indonesia **7**, 427 (2022).
38. K. a. A. M. J. Ketan, M.Sc Thesis, University of Baghdad, 2022.
39. F. S. Rocha, A. J. Gomes, C. N. Lunardi, S. Kaliaguine, and G. S. Patience, Canadian J. Chem. Eng. **96**, 2512 (2018).
40. K. A. Aadim, A. Z. Mohammad, and M. A. Abduljabbar, IOP Conference Series: Materials Science and Engineering **454**, 012028 (2018).
41. L. Kumaresan, G. Shanmugavelayutham, S. Surendran, and U. Sim, J. Korean Cer. Soci. **59**, 338 (2022).
42. A. Khodadadi, M. Farahmandjou, and M. Yaghoubi, Mat. Res. Exp. **6**, 025029 (2019).
43. D. Zhang, G. Mylsamy, X. Yang, Z. Xie, X. Su, F. Liang, B. Yang, and Y. Dai, Cer. Int. **47**, 16972 (2021).
44. J. Sokoloff, O. Pascal, T. Callegari, R. Pascaud, F. Pizarro, L. Liard, J. Lo, and A. Kallel, Comp. Rend. Phys. **15**, 468 (2014).
45. P. Peng, Y. Cheng, R. Hatzenbeller, M. Addy, N. Zhou, C. Schiappacasse, D. Chen, Y. Zhang, E. Anderson, Y. Liu, P. Chen, and R. Ruan, Int. J. Hydrogen En. **42**, 19056 (2017).

46. C. Han, R. Shi, D. Zhou, H. Li, L. Xu, T. Zhang, J. Li, F. Kang, G. Wang, and B. Li, ACS Appl. Mat. Inter. **11**, 15646 (2019).
47. M. I. Yousef, T. F. Mutar, and M. a. E. L. N. Kamel, Toxic. Rep. **6**, 336 (2019).
48. X. Tu and J. C. Whitehead, Int. J. Hydrogen En. **39**, 9658 (2014).
49. K. Wegner, B. Walker, S. Tsantilis, and S. E. Pratsinis, Chem. Eng. Sci. **57**, 1753 (2002).

تحضير وتوصيف أوكساید الألومنيوم المحضر بطريقتين مختلفتين للبلازما النفاثة

عبد الرحمن حامد شاكر[1] وكاظم عبد الواحد عادم[1]
[1]قسم الفيزياء، كلية العلوم، جامعة بغداد، بغداد، العراق

الخلاصة

في هذا البحث، تم استخدام نظام البلازما البارد تحت الضغط الجوي ويعمل بغاز الاركون بمعدل تدفق 2.5 لتر/دقيقة، وبزمن 4 دقائق مع جهد عالٍ 13.5 كيلو فولت وتغير في التيار بين المتردد المستمر لتكوين.AlO NPs من النتائج، عند استخدام التيار المستمر، وجد أن طيف الامتصاص يبدأ من 303 نانومتر وينخفض تدريجياً إلى 870 نانومتر. وعند التيار المتردد، كان عند 330 نانومتر ثم بدأ بالنزول إلى 902 نانومتر. لاحظ أن فجوة الطاقة عند التيار المستمر 3.49 eV أكبر من فجوة الطاقة عند التيار المتناوب.3.44 eV من خلال فحصXRD، وجد أن الطيف الناتج من الأشعة السينية غير متبلور ومطابق للنمط (42-1746). في (DC)، يبلغ متوسط حجم NPs المتكونة في فحص XRD (29.56)نانومتر وكان قريبًا جدًا مما ظهر في صور فحص FESEM حيث تراوح حجم الجسيمات النانوية الظاهرة بين (20- 50) نانومتر. في(AC) ، أعطى اختبارXRD حجمًا متوسطًا للجسيمات النانوية عند 38.21 نانومتر، بينما أظهرت صور مسح FESEM حجمًا يتراوح (20- 60) نانومتر، وهو قريب من اختبار XRD . بالنسبة للشكل الظاهر من صورFESEM ، أظهر أن جسيمات الالمنيوم النانوية كانت مجمعة ومترابطة، كل مجموعة متصلة بمجموعة أخرى. اما في(AC) ، فكانت الجسيمات النانوية شبه كروية، ممدودة قليلاً متصلة ببعضها البعض.

الكلمات المفاتحية: بلازما غير حرارية، جزيئات AlO النانوية، بلازما النفث، بلازما باردة AC DC، المجهر الإلكتروني الماسح للانبعاث الميداني